Unfolding and Conformational Studies on Bovine Adrenodoxin Probed by Engineered Intrinsic Tryptophan Fluorescence†

Frank Hannemann,‡,§ Aloke Kumar Bera,‡,§,|| Birgitta Fischer,§ Michael Lisurek,§ Klaus Teuchner,⊥ and Rita Bernhardt*,§

FR 8.8 Biochemie, Universität des Saarlandes, D-66041 Saarbrücken, Germany, and Max Born Institute for Nonlinear Optics and Short Time Spectroscopy, D-12489 Berlin, Germany

Received July 2, 2002

ABSTRACT: An intrinsic steady-state fluorescent system for bovine adrenodoxin has been developed to study the protein structure in solution and the processes involved in protein unfolding. Since mature Adx contains no natural Trp residue as internal probe, all of the aromatic amino acids, tyrosine at position 82 and four phenylalanines at positions 11, 43, 59 and 64, were at each case replaced by tryptophan. The resulting single tryptophan containing mutants kept their biological function compared with the wild type. Molecular modeling studies verify thermal unfolding experiments which point to a dramatically reduced stability caused by steric hindrance only for mutant F59W. Fluorescence spectra, Stern−Volmer quenching constants, and fluorescence energy transfer calculations indicated the analyzed positions to be situated in solution in the same immediate environment as in the crystal structure. Unfolding experiments with Gdn-HCl and time-resolved stopped-flow measurements provide evidence for differential stability and a chronologically ordered unfolding mechanism of the different fluorescence probe positions in the protein.

Bovine adrenodoxin (Adx)[1] is a single chain acidic iron−sulfur protein of the [2Fe-2S] type with a molecular mass of about 14 kDa. It functions as a central component in the electron transfer from NADPH-dependent adrenodoxin reductase (AdR) to the mitochondrial cytochromes P450 CYP11A1 and CYP11B1. CYP11A1 converts cholesterol to pregnenolone, the initial step in steroid hormone biosynthesis, and CYP11B1 catalyzes the 11β-hydroxylation of 11-deoxycorticosterone and 11-deoxycortisol and the production of aldosterone (*1*). The crystal structure of recombinant adrenodoxin (*2*, *3*) displays a compact ($\alpha + \beta$) fold typical for [2Fe-2S] ferredoxins, organized into a large core domain, containing the iron−sulfur cluster covered by a loop involved in redox partner binding (*4*), and a smaller interaction domain, comprising the acidic region responsible for the electrostatic interaction with positively charged residues on adrenodoxin reductase and CYP11A1 (*5*). Various investigations on wild-type and recombinant mutant Adx have been performed (*1*), most of them devoted to the interaction with its redox partners and to the elucidation of the mechanism of electron transfer. The general mechanism of electron transfer is still a matter of controversial discussion because different models for the transfer complex have been proposed (*1*, *5*, *6*).

Few studies have focused on the folding process of ferredoxins due to the destruction of the noncovalently attached iron−sulfur cluster prior to unfolding of the polypeptide chain under aerobic conditions (*7*, *8*). The reversible thermal unfolding of adrenodoxin was successfully studied in microcalorimetric studies under anaerobic conditions in a stabilizing reducing buffer system (*9*, *10*). Under these conditions the polypeptide follows a general reversible folding/unfolding transition described by a two-state model and shows relatively low conformational stability ($\Delta_d G$ about 21 kJ/mol at 25 °C and pH 8.5) compared with 25−60 kJ/mol for most of the globular proteins (*11*). Recently, the reversible unfolding of adrenodoxin under aerobic conditions in the presence of the reducing agent dithiothreitol has been reported (*12*). To facilitate unfolding and topological investigations of adrenodoxin, we replaced each of the five aromatic amino acids, phenylalanine in positions 11, 43, 59, and 64 and tyrosine in position 82, with tryptophan. Since Adx contains no tryptophan by nature, this strategy provided a protein with an efficient intrinsic fluorescence marker by single amino acid exchange. Substitutions of less fluorescent residues by tryptophans as reporter groups have been described previously for lactate dehydrogenase (*13*) and ribonucleases RNase A (*14*) and barnase (*15*) for unfolding studies.

The results of structural and unfolding measurements obtained in this study for the protein in solution will be discussed in comparison to the crystal structure of adrenodoxin (*2*, *3*).

† This work was supported by a fellowship from the DAAD to A.K.B., by the Deutsche Forschungsgemeinschaft (BE1343/12-1), and by the Fonds der Chemischen Industrie.

* To whom correspondence should be addressed. Phone: +49-681-302-3005. Fax: +49-681-302-4739. E-mail: ritabern@mx.uni-saarland.de.

‡ These authors contributed equally to the work.

§ Universität des Saarlandes.

|| Present address: Department of Biological Sciences, Purdue University, West Lafayette, IN 47907-1392.

⊥ Max Born Institute for Nonlinear Optics and Short Time Spectroscopy.

[1] Abbreviations: Adx, bovine adrenodoxin; AdR, bovine adrenodoxin reductase; CYP11A1, cytochrome $P450_{SCC}$; CYP11B1, cytochrome $P450_{11\beta}$; Gdn-HCl, guanidine hydrochloride; FPLC, fast performance liquid chromatography; CD, circular dichroism.

10.1021/bi020450z CCC: $22.00
Published on Web 08/13/2002

MATERIALS AND METHODS

Reagents and Biochemicals. Taq DNA polymerase and restriction endonucleases were purchased from Amersham Buchler KG. Horse heart cytochrome *c* and NADPH were obtained from Boehringer Mannheim, and Gdn-HCl was from Sigma. All reagents were of the highest purity grade commercially available.

Bacterial Strains, Plasmids, and Oligonucleotides. Escherichia coli strain BL21 was used as a host strain. Oligonucleotides containing the appropriate cloning sites and mutations were chemically synthesized by BioTez GmbH (Berlin). Mutations in the adrenodoxin cDNA in plasmid pKKHC were introduced by PCR and confirmed by plasmid cycle sequencing. All DNA manipulations were carried out using standard protocols (*16*).

Molecular Modeling. Amino acid exchanges were performed on the basis of the Adx crystal structure (*2*) with the program Insight II 97.0 (MSI, San Diego). Energy minimization was calculated using the program QUANTA 97 (MSI, San Diego) with 300 steps of steepest descents, and the overlay of the modeled mutant structures on the wild-type structure was carried out with the program Insight II 97.0.

Protein Purification. Recombinant adrenodoxin was purified after total lysis of *E. coli* cells according to the previously described procedure (*17*) with an additional chromatographic step on a FPLC Mono-Q 10/10 column (Pharmacia). The concentration of adrenodoxin was calculated using the extinction coefficient $\epsilon_{414} = 9.8$ (mM cm)$^{-1}$. Apoadrenodoxin was prepared by treatment of the native protein with trichloroacetic acid and dialysis against 10 mM potassium phosphate buffer, pH 7.4. An extinction coefficient $\epsilon_{276} = 3.0$ (mM cm)$^{-1}$ was assumed for wild-type apoadrenodoxin (*18*). According to the changed absorbance at 276 nm, $\epsilon_{276} = 4.2$ (mM cm)$^{-1}$ was used for mutant Y82W and $\epsilon_{276} = 4.6$ (mM cm)$^{-1}$ in the case of mutants F11W, F43W, F59W, and F64W to determine the concentration of the apoprotein. The isolation of recombinant adrenodoxin reductase from *E. coli*, as well as the estimation of the respective concentration, was carried out as described (*19*).

Thermal Stability. The characteristics of thermal unfolding of Adx wild type and mutants upon increasing temperatures were recorded as described previously (*20*) on a Jasco 715 spectropolarimeter fitted with a Jasco PTC348 temperature controller. Measurements were carried out at a heating rate of 50 °C/h from 20 to 60 °C with a temperature increment of 0.2 deg, monitoring the decrease of the maximum circular dichroism (CD) of the iron−sulfur cluster at 440 nm. The thermal transition temperature (T_m) was calculated from single wavelength CD scans with a nonlinear regression program using the two-state model.

Redox Potential Measurements. The redox potentials of adrenodoxin and the mutants were determined according to the photoreduction method (*21*) with the dye Safranin T as mediator and indicator as described (*20*). The data were analyzed according to the Nernst equation.

Cytochrome c Reduction Assay. The interaction of adrenodoxin and adrenodoxin reductase was assayed following the reduction of cytochrome *c* in a 33 mM potassium phosphate buffer (pH 7.4). The reaction was initiated by addition of NADPH. The absorption change at 550 nm was monitored, and the activity was determined using an extinction coefficient of $\epsilon_{550} = 20$ (mM cm)$^{-1}$ for cytochrome *c*.

UV/Visible and Fluorescence Measurements. Absorption spectra in the UV/visible region were measured at room temperature in a double-beam Shimadzu UV2100 spectrophotometer. Fluorescence emission spectra were recorded with a SPEX industries Fluoromax-2 spectrofluorometer with the excitation wavelength at 280 nm. The measurements were carried out at 20 °C in a buffer containing 50 mM Tris-HCl (pH 7.5). The excitation and emission bandwidths were 2.5 nm.

Acrylamide Quenching. Quenching experiments were carried out at an excitation wavelength of 295 nm. The protein concentration was 5.0 μM in 20 mM Tris-HCl, pH 7.5. Quenching accessibility was determined by successive addition of aliquots of a 5 M acrylamide stock solution. The fluorescence intensity was recorded at the previously determined λ_{max} of the native proteins. Fluorescence quenching data were fitted to the classical Stern−Volmer equation (*22*):

$$F_0/F = 1 + K_{SV}[Q] = 1 + k_q T_0[Q] \quad (1)$$

where F_0 and F are the fluorescence intensities in the absence and in the presence of the quencher, the product of $k_q T_0$ is referred to as the Stern−Volmer constant, k_q is the bimolecular rate constant, T_0 is the lifetime in the absence of the quencher, and [Q] is the molar concentration of the quencher. K_{SV} was calculated for each experiment by linear regression analysis. Since the Stern−Volmer quenching constants increase with increasing temperature, in our experiments the temperature was adjusted for each mutant.

Fluorescence Decay Investigations. Excitation was performed with the third harmonics (275 nm) of a Spectra Physics Ti:sapphire femtosecond laser Tsunami (repetition rate 80 MHz, pulse duration <100 fs). The emission was observed at a right angle to the excitation beam and imaged to the entrance slit of a monochromator (type, λ-scanner, Max Born Institute, Berlin; aperture, 1:3; wavelength range, 300−800 nm) fitted with a SPC 300 time-correlated single photon counting module (Becker & Hickl, Berlin) and a high-speed photomultiplier tube detector head PMH-100 (Becker Hickl, Berlin) equipped with a Hamamatsu H5783P-01 photosensor module. The data were numerically analyzed by deconvolution analysis with a sum of exponentials as the model function.

Energy Transfer and Distance Calculations. The presence of the chromophore [2Fe-2S] cluster together with a single tryptophan residue in each adrenodoxin mutant allows for distance determination according to Förster (*23*). Nonradiative energy transfer is defined as the transfer of excited-state energy from a donor to an acceptor and depends on the distance between these molecules or groups (*24*). The Förster theory defines the efficiency of energy transfer:

$$E = R_0^6/(R^6 + R_0^6) \quad (2)$$

where R_0, the distance at which the energy transfer efficiency is 50% (Förster distance), is given by

$$R_0 = (8.79 \times 10^{-25} \times J\kappa^2 Q_d n^{-4})^{1/6} \text{ (cm)} \quad (3)$$

κ^2, the orientation factor for dipole−dipole interaction, was assumed to be 0.67 for random orientation between the donor

and acceptor dipoles (*25*). Q_d is the quantum yield in the absence of energy acceptor, and *n* is the refractive index of the medium between donor and acceptor with a value of 1.4 for proteins (*24*). For energy transfer to occur, the fluorescence emission spectrum of the donor must overlap the absorption spectrum of the acceptor (Figure 3A, inset), as measured by the spectral overlap integral *J*:

$$J = [\int F(\lambda)\epsilon(\lambda)\lambda^4 \, d\lambda]/[\int F(\lambda) \, d\lambda] \quad (4)$$

where $F(\lambda)$ is the fluorescence intensity of the energy donor at wavelength λ, $\epsilon(\lambda)$ is the absorption coefficient (M^{-1} cm^{-1}) of the energy acceptor, and $d\lambda$ is the interval of measurement (1 nm).

The efficiency of energy transfer (*E*) was calculated from the quantum yield of the energy donor (Adx polypeptide) in the presence (Q_{da}) and absence (Q_d) of the energy acceptor, the [2Fe-2S] cluster (*26*):

$$E = 1 - Q_{da}/Q_d \quad (5)$$

The relative quantum yields were determined as follows:

$$Q_{sample} = Q_{std}(F_{sample}/F_{std})(I_{std}/I_{sample})(A_{std}/A_{sample}) \quad (6)$$

where *Q* is the relative quantum yield of the standard or sample, respectively, *F* is the fluorescence determined by integrating the area under the corrected fluorescence spectrum, *I* is the relative light intensity at the excitation wavelength, and *A* is the absorbance at the excitation wavelength (280 nm). In both cases the same excitation wavelength was used, and therefore $I_{std}/I_{sample} = 1$. In this measurement, mutant Adx was excited at 280 nm, and the emission was measured from 300 to 520 nm. In the case of Adx, 280 nm instead of 295 nm for Trp excitation can be used, since the Tyr fluorescence is significantly quenched, comprising less than 20% of the Trp fluorescence (Figure 3). The concentration of each protein was 5 μM. Tryptophan in water ($Q_{std} = 0.13$, excitation at 280 nm) was used as the quantum yield standard (*27*). The buffer background consisting of the water Raman band and contaminant fluorescence was subtracted from all measurements. For the phenylalanine mutants still containing their natural tyrosine residue, the wild-type Adx spectrum was used as a reference.

Equilibrium Unfolding Experiments. For all unfolding experiments, Adx solutions in 50 mM Tris-HCl (pH 7.5) and 2 mM dithiothreitol were adjusted to the desired final concentration of Gdn-HCl and incubated for 60 min at 20 °C. The parameters $\Delta G°_u$ (free energy of unfolding in the absence of denaturant), *m* (cooperativity of unfolding), and C_m (midpoint concentration of denaturant required to unfold half of the protein) were obtained as previously outlined (*28*) using the equations:

$$\Delta G_u = -RT \ln K_u \quad (7)$$

and

$$\Delta G_u = \Delta G°_u - m[\text{Gdn-HCl}] \quad (8)$$

Kinetic Measurements of Adrenodoxin Unfolding. All kinetic fluorescence experiments were performed at 20 °C on an Applied Photophysics stopped-flow SX17MV system. Unfolding was initiated by mixing the native protein (4 μM Adx, 4 mM dithiothreitol) and the denaturant (8 M Gdn-HCl), both solutions in 50 mM Tris-HCl, pH 7.0, with a 1:1 volume ratio. Unfolding kinetics were recorded as a function of time with the intensity measured at 90° to the excitation wavelength (280 nm) after passing through a 320 nm cutoff filter. Measurements were repeated three to five times at a given condition to ensure reproducibility. The reaction traces were overlaid, and the averaged curves were fitted to double- or triple-exponential functions to determine apparent rate constants and amplitudes.

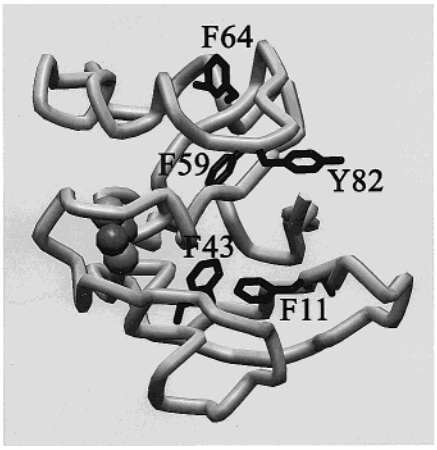

FIGURE 1: Three-dimensional structure of bovine Adx (*2*), showing the position of the residues that were mutated in black. Residues Tyr82, Phe64, and Phe59 are part of the interaction domain, and residues Phe43 and Phe11 are situated in the iron−sulfur cluster containing core domain. The figure was generated using the program WebLab Viewer (MSI, San Diego).

RESULTS

Molecular Modeling. Each aromatic residue in bovine Adx (Figure 1) was changed to Trp by site-directed mutagenesis. Since a Trp requires more space than a Phe or Tyr residue, molecular models of the five resulting single tryptophan containing substitution mutants F11W, F43W, F59W, F64W, and Y82W were created. Figure 2 shows the close-up view on the described residues in the corresponding structures of the wild type and the five mutants on the basis of the Adx crystal structure. After energy minimization the Trp residues can be inserted into the positions previously occupied by Phe or Tyr with minimal changes in orientation of the indole ring. Only the tryptophan in mutant F59W seems to be in very close range to the proximate residues Met100, Met103, and Leu29, indicating some steric interference. Consequences for the global structure and for the stability of the other mutants induced by the integrated Trp residues were not obvious from the molecular modeling study.

Protein Expression and Purification. All mutant proteins have been produced in *E. coli* and purified to homogeneity. The recombinant proteins show a correct assembly of the [2Fe-2S] cluster confirmed by the absorption spectra in the visible region, which were indistinguishable from the wild-type protein spectrum (data not shown). A high purification level is indicated by the absorbance ratio A_{414}/A_{276} for wild-type Adx of 0.92 and for the mutants between 0.66 and 0.60 due to the presence of tryptophan, which increases the absorbance in the near-UV region around 280 nm.

Biological Activity. The redox potential and the electron transfer ability of the mutants were investigated to prove

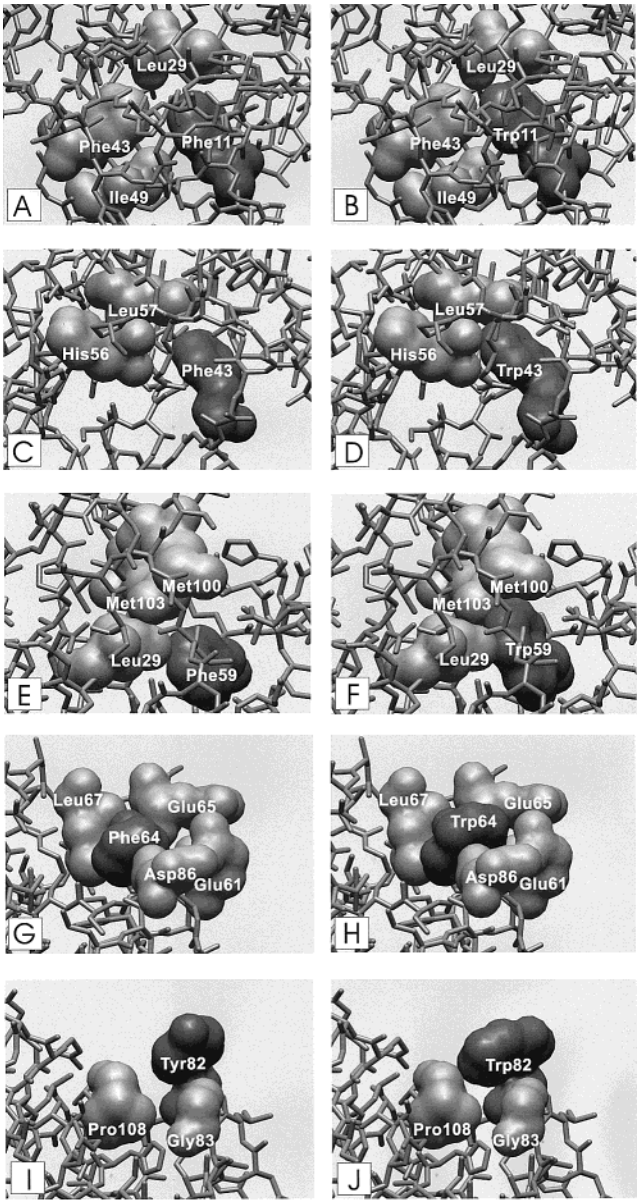

FIGURE 2: Close-up view of the three-dimensional structure of Adx in the vicinity of the mutated positions and the corresponding wild-type (A) Phe11, (B) Trp11, (C) Phe43, (D) Trp43, (E) Phe59, (F) Trp59, G) Phe64, (H) Trp64, (I) Tyr82, and (J) Trp82. Surfaces of the selected amino acids are shown on the basis of the van der Waals radius of each atom. The figure was generated using the program WebLab Viewer (MSI, San Diego).

whether the biological function of the proteins was affected by the mutations (Table 1). The redox potential of mutant Y82W is only slightly increased (−258 mV) compared with the wild type (−274 mV). Mutants F11W, F43W, F59W, and F64W show redox potentials similar to that of wild type within a variance of 10 mV, indicating that structural parameters in the vicinity of the iron−sulfur cluster influencing the redox properties of the protein are not disturbed. The catalytic activity of mutant proteins was measured following the NADPH-dependent cytochrome *c* reduction (Table 1), which reflects the electron transfer velocity from AdR to Adx. Under the conditions employed, cytochrome *c* is in large excess, and the derived K_m values are essentially equivalent to dissociation constants (K_d) of the AdR−Adx complex (*29*). The replacement mutants demonstrated no significant changes either in their electron transfer (υ_{max}) or

Table 1: Biological Activity Parameters of Wild-Type Adx and Different Mutants

proteins	cytochrome *c* assay[a]		redox potential[a] (mV)
	K_m (nM)	υ_{max}[b]	
wild type	23.9	90.9	−274
F11W	29.5	68.9	−277
F43W	24.9	77.5	−268
F59W	21.3	95.8	−268
F64W	25.4	95.2	−267
Y82W	26.1	95.2	−258

[a] Relative deviations in cytochrome *c* assays were 5%; standard deviations for redox potentials were ±5 mV. [b] Expressed as nmol of cytochrome *c* reduced/min.

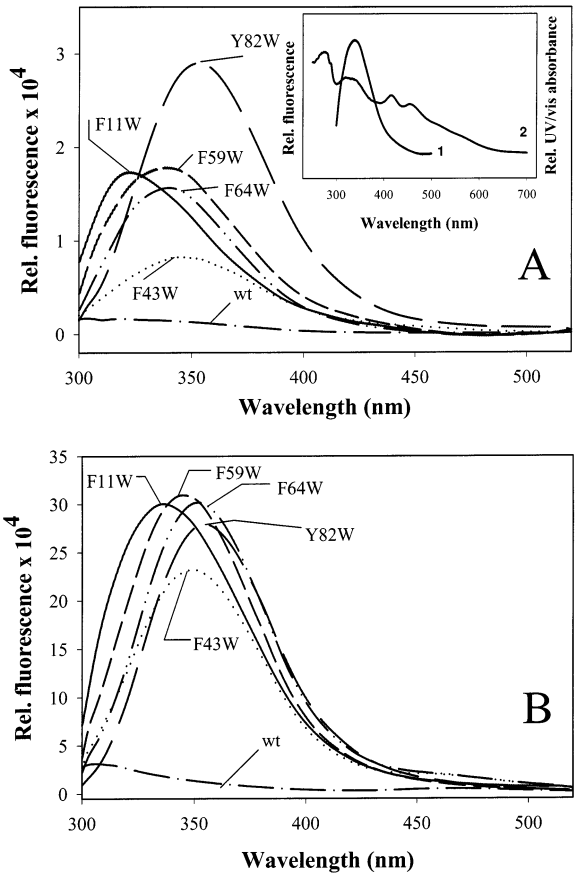

FIGURE 3: Fluorescence emission spectra of wild-type Adx (dash dot) and the mutants F11W (solid), F43W (dotted), F59W (short dash), F64W (dash dot dot), and Y82W (long dash) in their holo forms (A) and their apo forms (B). Spectra of mutants F11W, F43W, F59W, and F64W were corrected for the wild-type Adx spectrum, and wild-type and Y82W spectra were corrected for buffer as a reference. The representative donor/acceptor spectral overlap between fluorescence emission (1) and UV/vis absorbance (2) is shown as an inset for the mutant F64W.

in their interaction properties (K_m) when compared with wild-type Adx. Thus, the functional tests described confirm that the amino acid exchange in all mutants does not affect their functional activity.

Fluorescence Measurements of Trp Mutants. The presence of Trp residues in the Adx mutants was confirmed by the steady-state fluorescence emission spectra of the apo and holo forms of these mutants (Figure 3). The maximum emission wavelength (λ_{max}) of the holoprotein spectrum is characteristic for the environment of the tryptophan residues in Adx in solution. The residues in positions 43 (λ_{max} at 345

Table 2: Fluorescence Lifetime, Quenching Constants, and Fluorescence Energy Transfer Determination of Adx Mutants[a]

mutant	τ (ns)	K_{SV} (M^{-1})	k_q ($\times 10^9$ M^{-1} s^{-1})	Q_H	Q_A	E	$J \times 10^{14}$	R_{obs} (nm)	R_c (nm)
F11W	1.51	1.16	0.81	0.0017	0.117	0.985	1.74	1.29	1.35
F43W	1.54	1.74	1.20	0.0010	0.085	0.998	1.87	1.19	0.85
F59W	0.924	1.81	2.10	0.0020	0.112	0.981	1.77	1.33	1.45
F64W	0.95	1.45	1.68	0.0017	0.121	0.985	1.88	1.30	1.83
Y82W	0.81	1.97	2.54	0.0032	0.125	0.974	0.89	1.45	1.52

[a] The abbreviations represent the mean fluorescence lifetime (τ), the Stern−Volmer constant (K_{SV}), the dynamic quenching constant (k_q), the quantum yield Q_H for holoprotein and Q_A for apoprotein, the efficiency of energy transfer (E), the overlap integral (J), and the distance between the tryptophan residue and the [2Fe-2S] cluster on the basis of Förster energy transfer calculations (R_{obs}) and on the basis of the crystal structure (R_c).

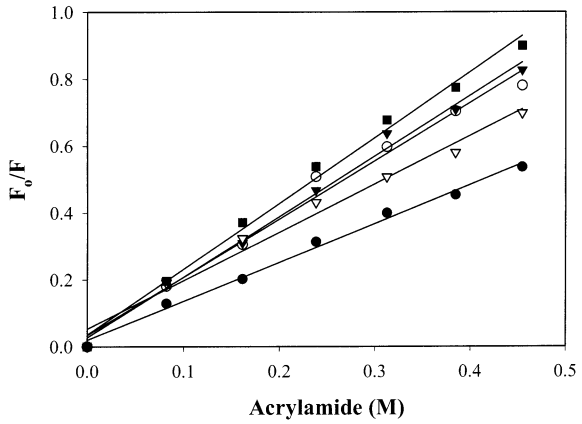

FIGURE 4: Stern−Volmer plot for acrylamide quenching of the tryptophan fluorescence of Adx mutants. Proteins F11W (closed circle), F43W (open circle), F59W (closed triangle) F64W (open triangle), and Y82W (closed squere) were titrated with acrylamide, and the fluorescence integral (λ_{ex} = 295 nm; λ_{em} = 300−520 nm) was calculated after each addition.

nm), 59 (340 nm), and 64 (339 nm) are located in the protein core in a less hydrophobic surrounding than the tryptophan in position 11. The emission maximum of this mutant (325 nm) indicates an extreme blue shift of the emission band, which comes close to the value of 320 nm reported for free tryptophan in hexane, suggesting a location in a nonpolar environment in the protein core. The maximum emission wavelength of 352 nm for the tryptophan in position 82 is characteristic for a residue situated in a polar environment on the protein surface.

Further studies were performed on the surroundings of the aromatic residues by studying the quenching of the intrinsic Trp fluorescence. The indole fluorescence in all mutant proteins can be quenched by acrylamide, indicating that the tryptophan reporter positions are accessible to the small, uncharged, water-soluble molecule. In addition, fluorescence decay spectra were recorded to allow the complete analysis of steady-state fluorescence quenching data. Decay spectra of all mutants were best fitted with a two-term model. The mean lifetimes are summarized in Table 2.

The Stern−Volmer Plot was linear for all five mutants, indicating a similar type of fluorescence quenching in all cases (Figure 4). The slope of the plot increased with higher temperatures, which seems to be due to a dynamic quenching mechanism which is the general feature observed for tryptophanyl fluorescence quenching by acrylamide (*30*). According to eq 1, the Stern−Volmer constants (K_{SV}) and the dynamic quenching constants (k_q) for the proteins were determined (Table 2). F11W is very poorly quenched by acrylamide, indicating an almost inaccessible location of the tryptophan in the hydrophobic core. The Trp fluorescence of the mutants F43W, F59W, and F64W was moderately quenched by acrylamide. The highest quenching constant was observed for Y82W, characteristic for an accessible position on the surface of the molecule.

The distance (R_{obs}) between the tryptophan residues and the [2Fe-2S] cluster was estimated on the basis of fluorescence energy transfer measurements (*23*). Averaged distances (R_c) were also calculated on the basis of the crystal structure between the four atoms of the cluster and the atom Cγ of the respective aromatic residue. The comparison of the distance values R_{obs} and R_c shows only slight deviations in the case of the core domain mutants F43W and F64W (Table 2), which can be caused by using the same assumed orientation factor for all molecule positions during the calculation of the distances.

Taken together, the microenvironment, solvent accessibility, and distance to the cluster of all analyzed positions that can be deduced from fluorescence measurements for the protein in solution are similar to the positions found in the crystal structure (Figure 1).

Thermal Stability. For analysis of the influence of Trp mutations on the conformational stability of the proteins, the integrity of the iron−sulfur cluster was measured by CD spectroscopy during thermal unfolding. The CD signal of melting curves recorded at the maximal CD signal (at 440 nm) of the cluster reveals that mutant F59W shows, in coincidence with the molecular modeling study, a significantly lower thermal stability (Figure 5A). The thermal transition temperature (T_m) of this mutant is lowered by 14 °C whereas all other mutants and the wild type display T_m values within a range of 5 °C (Table 3).

Equilibrium Unfolding. The change of the microenvironment of the tryptophan residues as a function of the Gdn-HCl concentration was investigated by two approaches: determination of the emission maxima and integration of the fluorescence intensity in the region of 300−520. Both approaches yielded similar thermodynamic parameters (Table 3) for the free energy of unfolding ($\Delta G°_u$), for the cooperativity of unfolding (m), and for the midpoint concentration of denaturant required to unfold half of the protein (C_m). Upon an increase of the Gdn-HCl concentration, the emission maximum of all mutants shifted to 358 nm (data not shown). This red shift generally reflects the transfer of a Trp residue to a more polar environment. In the case of F59W, the red shift begins at relatively low concentrations of the denaturant, indicating an immediate microenvironment change at this position which is expected for a mutant that has a reduced overall stability. The change of the integrated fluorescence intensity as a function of the Gdn-HCl concentration for the

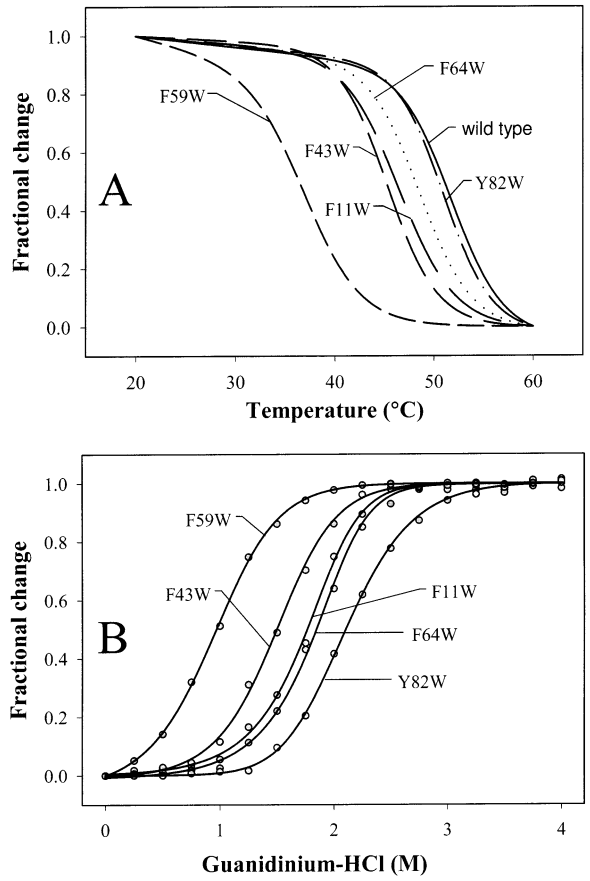

FIGURE 5: Denaturation curves of Adx and Trp mutants of Adx. Thermal denaturation (A) of wild-type Adx (solid), F11W (long dash), F43W (medium dash), F59W (short dash), F64W (dotted), and Y82W (dash dot) was followed in a glycine buffer system (pH 8.5) containing 2-mercaptoethanol, Na_2S, and ascorbic acid. Single wavelength melting curves have been recorded by CD spectroscopy at 440 nm. Equilibrium Gdn-HCl unfolding (B) transitions of the mutants monitored by steady-state fluorescence. The fraction of unfolded protein at each Gdn-HCl concentration, calculated from the integration of the fluorescence intensity in the region of 300−520 nm, is plotted as a function of denaturant concentration.

Table 3: Thermodynamic Unfolding Parameters Measured by Equilibrium Gdn-HCl Denaturation and Thermal Denaturation[a]

proteins	$\Delta G°_u$ (kJ mol^{-1})	m (kJ mol^{-1} M^{-1})	C_m (M)	T_m (°C)
wild type				51.9
F11W	15.44	8.96	1.72	46.6
F43W	13.73	9.15	1.50	45.4
F59W	8.86	8.74	1.01	37.3
F64W	17.44	9.55	1.82	48.7
Y82W	18.79	8.72	2.15	51.2

[a] The parameters $\Delta G°_u$ (free energy of unfolding in the absence of denaturant), m (cooperativity of unfolding), and C_m (midpoint concentration of denaturant required to unfold half of the protein) were determined by Gdn-HCl denaturation and from the integration of the fluorescence intensity; the transition temperature T_m was calculated from thermal denaturation experiments. The maximal standard deviations for T_m were ±0.2 °C.

five mutants is shown in Figure 5B. The protein structure reacts very sensitively to the slightest concentration changes in the lower concentration range between 1 and 2 M where the strongest effects on emission changes are observed. At the concentration range around and beyond 4 M, however, no radical changes could be visualized. All mutants show smooth transition curves indicating a cooperative unfolding

Table 4: Kinetic Parameters[a] of Trp Fluorescence during Unfolding of Adx Mutants

mutant	k_{app1}	rel amp$_1$	k_{app2}	rel amp$_2$	k_{app3}	rel amp$_3$
F11W	1.84	0.87	0.0037	0.13		
F43W	1.34	0.13	0.0035	0.87		
F64W	1.50	0.14	0.0037	0.86		
Y82W	0.34	0.18	0.03	0.29	0.0043	0.53

[a] Data for the apparent rate constants (k_{app} in s^{-1}) and amplitudes (amp, normalized to a sum of 1) for the different processes were obtained for F11W, F43W, and F64W by double-exponential fits and for Y82W by triple-exponential fits using the least-squares method.

event. In terms of the local denaturation values $\Delta G°_u$, the Trp residues in positions 43, 11, 64, and 82 feature stabilities within the range between 15.4 and 18.8 kJ mol^{-1}, whereas the value for position 59 is dramatically reduced by a factor of 2 (Table 3).

Kinetics of Protein Unfolding. A time-resolved unfolding analysis for the mutants F11W, F43W, F64W, and Y82W was performed using stopped-flow experiments. Due to its instability, mutant F59W was not further analyzed. Solutions of the mutants were rapidly mixed with a Gdn-HCl solution to a final concentration of the denaturant of 4 M, and the fluorescence signals were recorded for 1000 s (Figure 6). For the analysis different kinetic models have been applied, and the residuals for the best fits are presented. The fits show still errors indicating that adrenodoxin unfolding does not follow exactly the classical kinetics as obtained for model proteins. The time course of unfolding derived from stopped-flow experiments of mutants F11W, F43W, and F64W was best fitted to a double-exponential process, consisting of a fast phase followed by a slower one. The time course of mutant Y82W was best fitted to a triple-exponential process. For this mutant an additional phase can be observed between the fast phase and slow phase. The slow phase shows similar rate constants for all mutants. The unfolding rate constants and amplitudes for the different phases are summarized in Table 4. Positions 11, 64, and 82 reach an amplitude after 1000 s in the same relative fluorescence intensity range between 2900 and 3100. According to the close location to the cluster the value for the final amplitude of mutant F43W (2000) is significantly lower. The largest k_{app1} values for the first unfolding phase can be observed for position 11 (Figure 6A). The regions around positions 64 and 43 (Figure 6D) show significantly lower k_{app1} values than position 11, and the value for the region of residue 82 was 5.4 times reduced compared to residue 11.

DISCUSSION

The purpose of this study was to investigate the local conformation at different positions in Adx in its soluble form and to derive structural information during the unfolding processes of the protein. To get access to different regions in the Adx molecule, tryptophan as an intrinsic fluorescence marker was introduced by site-directed mutagenesis in positions previously occupied by less fluorescent aromatic amino acids. Figure 1 shows the location of the mutated residues mapped on the protein backbone of the crystal structure. The aromatic residues Tyr82, Phe64, and Phe59 are part of the interaction domain, whereas Tyr82 is solvent exposed and positioned at one edge of this domain. Phe59 and Phe64 are part of a hydrophobic cluster connecting the

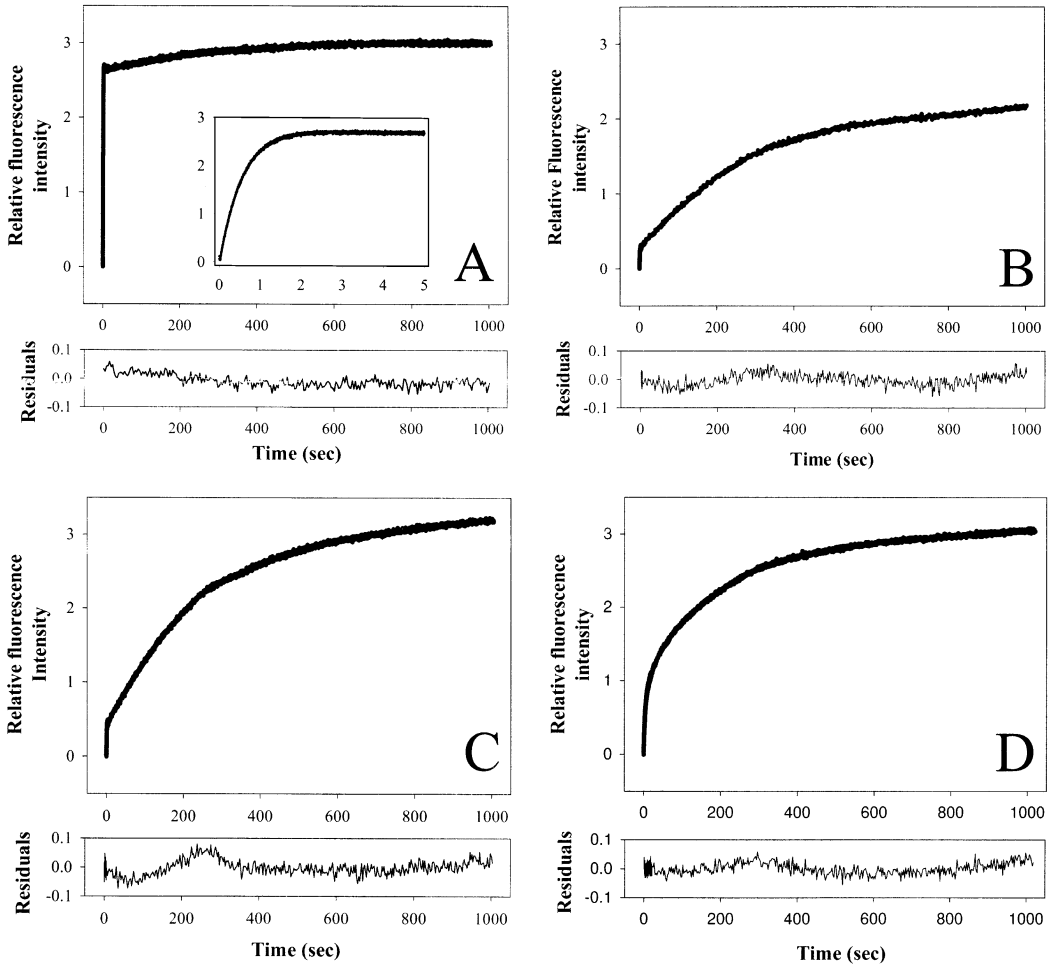

FIGURE 6: Unfolding time course of mutants F11W (A), F43W (B), F64W (C), and Y82W (D) measured by fluorescence stopped-flow experiments. Unfolding was initiated by rapid mixing of the sample with an 8 M Gdn-HCl solution. The inset of (A) shows the intensity change in the first 5 s. The unfolding kinetic traces were fitted with a double-exponential function for (A), (B), and (C) and with a triple-exponential function for (D). The residuals of each fit are shown on the bottom of the corresponding kinetic trace.

interaction domain with the large hydrophobic cluster of the core domain. Phe11 is located in the hydrophobic cluster of the core domain, and residue Phe43 is a member of a group of amino acids which are wrapped around the iron−sulfur cluster (*2*).

The indicated positions of the aromatic residues in the protein structure in solution have been analyzed in this study by steady-state intrinsic Trp fluorescence measurements. Fluorescence spectra as well as acrylamide quenching experiments and distance calculations based on Förster energy transfer measurements indicate that the aromatic residues in positions 11, 43, 59, 64, and 82 are located in the same local conformation and distance to the iron−sulfur cluster as presented in the crystal structure (*2*). The calculated distance values show slight differences compared to the crystal structure but range within the error margin of the less exact method of fluorescence-based calculations.

The replacement of aromatic residues Phe and Tyr by the larger amino acid Trp did not influence the biological function of the mutants as electron transfer proteins. The properties of the iron−sulfur cluster, the redox potential and the ability to transfer electrons, are preserved in all mutants. These results are in agreement with previous studies, because the mutated residues are not participating in the direct recognition of the Adx partner proteins, involving the acidic amino acids in the domain between Glu69 and Asp86 (*5*) or the iron−sulfur loop region (*4*) and are not located in the calculated electron pathway of Adx (*31*). Moreover, the molecular models of the mutant proteins reveal that the larger side chain of Trp can be integrated in positions 11, 43, 64, and 82 with no steric hindrance. Only the van der Waals radii of the Trp in mutant F59W interfere with those of the proximate residues Met100, Met103, and Leu29. The molecular modeling results were confirmed by thermal denaturation studies which show that only mutant F59W has a significantly lower thermal stability (Figure 5). On the basis of the thermal unfolding experiments, all results obtained by fluorescence measurements during unfolding studies with mutant F59W have to be carefully discussed in light of the lower stability of this protein. In all other mutants, F11W, F43W, F64W, and Y82W, steric differences after substitution of the respective aromatic amino acid by Trp have no significant consequences for the stability of the protein. These mutants represent therefore suitable molecules for structural and unfolding investigations of different regions in the Adx polypeptide using their intrinsic fluorescence properties.

The equilibrium unfolding process of bovine Adx monitored by fluorescence spectroscopy of the molecule was in all cases monophasic (Figure 3). In the simplest model that describes the experimental observations it can be assumed that the protein exists in the native or in the denatured state. These results strongly support a cooperative two-state

Scheme 1: Proposed Model for Protein Unfolding in Adx[a]

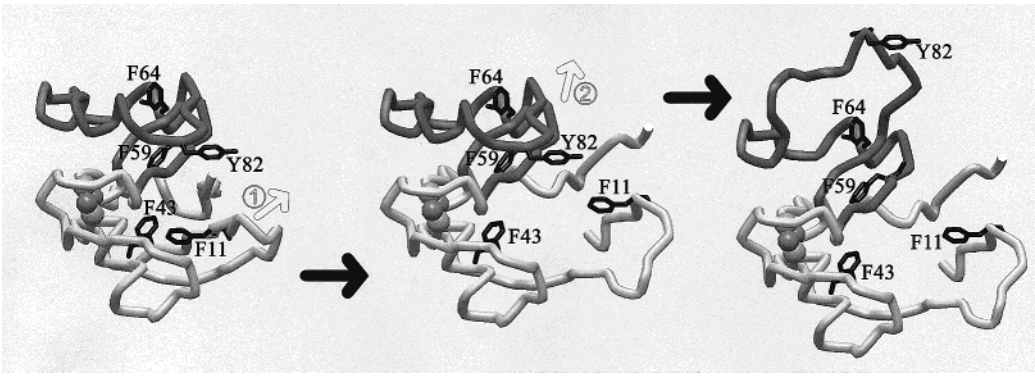

[a] The illustration was generated manually using the program WebLab Viewer (MSI, San Diego). The core domain is drawn in light gray and the recognition domain in dark gray. The probable unfolding processes suggested in the Discussion representing the first fast unfolding of the core domain position 11 (1) and the recognition domain position 82 (2) are indicated by arrows.

unfolding of all analyzed mutants in both the interaction domain (Trp64, Trp82) and the core domain (Trp11, Trp43, Trp59) and are therefore subject to the same overall folding process as described earlier for the Adx molecule measured by microcalorimetry (*9*) and CD spectroscopy (*20*). The ΔG values for the free energy of unfolding of mutants in positions 11, 43, 64, and 82 are in the range between 15.4 and 18.8 kJ mol^{-1} (Table 3), being in good agreement with the value of 18.8 kJ mol^{-1} obtained previously for the wild type by pressure-induced unfolding (*32*).

The unfolding kinetics of the four Trp mutants analyzed in the presence of 4 M Gdn-HCl indicate the existence of transient protein conformations during the transition from the native conformation to the unfolded state, representing a more complex unfolding reaction also reported for nuclease barstar (*33*) or the small iron−sulfur protein rubredoxin (*34*). This interesting extension of the unfolding process observed in iron−sulfur proteins seems to be induced by the presence of two protein domains and a quenching cofactor, resulting during the unfolding of Adx in at least biphasic fluorescence time courses which are dependent on the accessibility of the Trp reporter residues to the solvent and on the distance to the quenching iron−sulfur cluster. Moreover, the unusual kinetic heterogeneity of the different positions in the Adx molecule indicates a differentiated unfolding of the analyzed protein positions in the first fast unfolding process. The following model of the Adx unfolding can be outlined. Scheme 1 shows a manually arranged sketch illustrating the fast unfolding processes measured for positions 11 and 82. Position 11 localized in a hydrophobic environment of the Adx core is shielded by three β-strands and is stabilized by hydrophobic interactions of Pro108 with Ile58, His56, and Tyr82 and hydrogen bonds between Val107 and Ile12, Arg106 and Ile58, and the hydrogen bond between residues Pro108 and Arg14, which plays an important role for the overall protein stability (*35*, *36*). The loss of this connection between the N- and C-terminus of the protein induced under denaturing conditions leads to an immediate solvent accessibility of the buried Trp residue 11 at the N-terminus represented by the fastest first unfolding process of all analyzed positions. The amplitude of the rapid first phase of this position reaches 80% of the maximal fluorescence range in the first 5 s. The fluorescence properties of the reporter in position 82 as an already solvent-exposed part of the interaction domain (Figure 1) are, in contrast to the other positions, primarily a function of the distance to the quenching iron−sulfur cluster. The first rapid unfolding phase of position 82 shows a lower k_{app1} value than that of the other positions (Table 4). Even though viewed over the measured time period of 1000 s, the time for half-maximal unfolding indicates that position 82 (60 s) unfolds next to position 11 (0.5 s) and before positions 64 (143 s) and 43 (167 s). The first two unfolding processes indicated by position 82 can be a sensor for the unfolding of the interaction helix and the opening of a cleft between the interaction helix and the core of the protein induced by the loss of the salt bridge between Arg89 and Glu74 (Grinberg and Bernhardt, submitted results) and the structure stabilizing hydrogen bonds His56 to Trp82 and to Ser88 (*2*). The positions of Trp64 in the hydrophobic part of the interaction domain and of Trp43 in the hydrophobic core around the iron−sulfur cluster are additionally stabilized by hydrophobic interactions and show a slower unfolding characteristic indicated by lower values for k_{app1} and amp_1 for the first rapid unfolding phase compared with position 11 (Figure 5, Table 4). All analyzed positions show a similar k_{app} value for the final phase of the unfolding kinetics which is likely to be generated by the uncovering of the iron−sulfur cluster, which remains associated to the unfolded protein as reported earlier (*12*). The lowest final amplitude of the unfolding process for position 43 suggests that the cluster remains coordinated close to this position. In the most probable complex under the conditions applied the iron−sulfur cluster is coordinated via the natural ligands Cys46 and Cys52 and the thiol groups of DTT and forms a sterically favorable cyclic structure analogue to that of chemically synthesized cluster complexes (*37*).

In conclusion, five biofunctional mutants of the adrenal bovine Adx were constructed by exchanging phenylalanine or tyrosine for tryptophan. The intrinsic fluorescence of the generated tryptophan residues in the recombinant iron−sulfur proteins proved a valuable and convenient system for structural studies. Local conformation states related to the immediate environment of the mutations and the distances to the iron−sulfur cluster were presented. All data were in agreement with the structural properties derived from the crystal structure of Adx. Steady-state and time-resolved unfolding studies provided for the first time information about the unfolding process and the dynamics of solvent exposure at different positions of the protein and could be

of importance for unfolding/folding studies of other ferredoxins.

ACKNOWLEDGMENT

The authors thank Wolfgang Reinle for excellent technical assistance in purification of the proteins, Martin Kiefer for competent support during stopped-flow measurements, and Reinhard Lange and Wolfgang Pfeil for critical reading of the manuscript and for helpful comments.

REFERENCES

1. Grinberg, A. V., Hannemann, F., Schiffler, B., Müller, J. J., Heinemann, U., and Bernhardt, R. (2000) *Proteins 40*, 590−612.
2. Müller, A., Müller, J. J., Müller, Y. A., Uhlmann, H., Bernhardt, R., and Heinemann, U. (1998) *Structure 6*, 269−280.
3. Pikuleva, I. A., Tesh, K., Waterman, M. R., and Kim, Y. (2000) *Arch. Biochem. Biophys. 373*, 44−55.
4. Hannemann, F., Rottmann, M., Schiffler, B., Zapp, J., and Bernhardt, R. (2001) *J. Biol. Chem. 276*, 1369−1375.
5. Vickery, L. E. (1997) *Steroids 62*, 124−127.
6. Bernhardt, R. (1996) *Rev. Physiol. Biochem. Pharmacol. 127*, 137−221.
7. Padmanabhan, R., and Kimura, T. (1970) *J. Biol. Chem. 245*, 2469−2475.
8. Petering, D. H., and Palmer, G. (1970) *Arch. Biochem. Biophys. 141*, 456−464.
9. Burova, T. V., Bernhardt, R., and Pfeil, W. (1995) *Protein Sci. 4*, 909−916.
10. Burova, T. V., Beckert, V., Uhlmann, H., Ristau, O., Bernhardt, R., and Pfeil, W. (1996) *Protein Sci. 5*, 1890−1897.
11. Privalov, P. L. (1979) *Adv. Protein Chem. 33*, 167−241.
12. Bera, A. K., Grinberg, A., and Bernhardt, R. (1999) *Arch. Biochem. Biophys. 361*, 315−322.
13. Smith, C. J., Clarke, A. R., Chia, W. N., Irons, L. I., Atkinson, T., and Holbrook, J. J. (1991) *Biochemistry 30*, 1028−1036.
14. Torrent, J., Connelly, J. P., Coll, M. G., Ribo, M., Lange, R., and Vilanova, M. (1999) *Biochemistry 38*, 15952−15961.
15. Loewenthal, R., Sancho, J., and Fersht, A. R. (1991) *Biochemistry 30*, 6775−6779.
16. Sambrook, J., Fritsch, E. F., and Maniatis, T. (1989) *Molecular Cloning. A Laboratory Manual*, 2nd ed., Cold Spring Harbor Laboratory Press, Cold Spring Harbor, NY.
17. Uhlmann, H., Beckert, V., Schwarz, D., and Bernhardt, R. (1992) *Biochem. Biophys. Res. Commun. 188*, 1131−1138.
18. Lim, B. T., and Kimura, T. (1980) *J. Biol. Chem. 255*, 2440−2444.
19. Sagara, Y., Wada, A., Takata, Y., Waterman, M. R., Sekimizu, K., and Horiuchi, T. (1993) *Biol. Pharm. Bull. 16*, 627−630.
20. Uhlmann, H., and Bernhardt, R. (1995) *J. Biol. Chem. 270*, 29959−29966.
21. Sligar, S. G., and Gunsalus, I. C. (1976) *Proc. Natl. Acad. Sci. U.S.A. 73*, 1078−1082.
22. Eftink, M. R., and Ghiron, C. A. (1976) *Biochemistry 15*, 672−680.
23. Förster, T. (1948) *Ann. Phys. 2*, 55−75.
24. Stryer, L. (1978) *Annu. Rev. Biochem. 47*, 819−846.
25. Haas, E., Katchalski Katzir, E., and Steinberg, I. Z. (1978) *Biochemistry 17*, 5064−5070.
26. Cheung, H. C. (1991) in *Topics in Fluorescence Spectroscopy* (Lakowicz, J. R., Ed.) pp 127−176, Plenum Publishing, New York.
27. Tatischeff, I., and Klein, R. (1975) *Photochem. Photobiol. 22*, 221−229.
28. Pace, C. N. (1995) *Methods Enzymol. 259*, 538−554.
29. Lambeth, J. D., and Kamin, H. (1979) *J. Biol. Chem. 254*, 2766−2774.
30. Eftink, M. R., and Ghiron, C. A. (1981) *Anal. Biochem. 114*, 199−227.
31. Müller, J. J., Müller, A., Rottmann, M., Bernhardt, R., and Heinemann, U. (1999) *J. Mol. Biol. 294*, 501−513.
32. Lange, R., Bec, N., Mozhaev, V. V., and Frank, J. (1996) *Eur. Biophys. J. 24*, 284−292.
33. Agashe, V. R., Schmid, F. X., and Udgaonkar, J. B. (1997) *Biochemistry 36*, 12288−12295.
34. Cavagnero, S., Zhou, Z. H., Adams, M. W., and Chan, S. I. (1998) *Biochemistry 37*, 3377−3385.
35. Grinberg, A. V., and Bernhardt, R. (1998) *Protein Eng. 11*, 1057−1064.
36. Grinberg, A., and Bernhardt, R. (1998) *Biochem. Biophys. Res. Commun. 249*, 933−937.
37. Mayerle, J. J., Denmark, S. E., Depamphilis, B. V., Ibers, J. A., and Holm, R. H. (1975) *J. Am. Chem. Soc. 97*, 1032−1045.

BI020450Z